Received: 29 May 2018 | Revised: 27 February 2019 | Accepted: 12 March 2019
DOI: 10.1002/we.2342

WILEY

RESEARCH ARTICLE

Spatiotemporal variability of the wind power resource in Argentina and Uruguay

Emilio Bianchi | **Andrés Solarte** | **Tomás Guozden**

Laboratorio de Procesamiento de Señales Aplicadas y Computación de Alto Rendimiento, Universidad Nacional de Río Negro, San Carlos de Bariloche, Argentina

Correspondence
Emilio Bianchi, Mitre 630, Laboratorio de Procesamiento de Señales Aplicadas y Computación de Alto Rendimiento, Universidad Nacional de Río Negro, San Carlos de Bariloche, Río Negro, Argentina.
Email: ebianchi@unrn.edu.ar

Funding information
Fondo para la Investigación Científica y Tecnológica; Universidad Nacional de Rio Negro

Abstract

The spatiotemporal variability of the wind power resource over Argentina and Uruguay is assessed based on the Modern-Era Retrospective Analysis for Research and Applications 2 (MERRA2) dataset. Hourly wind speeds were interpolated to 100-m height, and then, wind power outputs were computed using power curves of three International Electrotechnical Commission (IEC) wind classes. The time series of wind power outputs were filtered using a fast Fourier transform (FFT) to separate regular (annual and daily) from irregular (interannual and synoptic scale) cycles. An empirical orthogonal function analysis was applied to the resulting datasets to obtain the main modes of variability. The results show that the combination of wind power outputs from southern and northern Patagonia broadly follows the average annual electric load. Patagonia exhibits the highest variability on the interannual, annual, and synoptic timescales. On the interannual and synoptic timescales, the variability modes are associated with known and distinct atmospheric circulation modes. The interannual modes of variability are associated with opposite surface level pressure (SLP) anomalies between middle and high latitudes.

KEYWORDS

Argentina, EOF, Uruguay, variability, wind power

1 | INTRODUCTION

Wind energy is considered a nondispatchable energy source[1-3] because of its high variability and to the fact that it depends on changing meteorological conditions.[4-6] This characteristic of wind power can negatively affect the stability and reliability of power grids[7-9] and increase the costs and complexity of the operation of the electric system and the usage of backup reserves.[4,10,11]

The variability of wind speeds, and hence wind power production, operates over different timescales.[11,12] The most important timescales of variability of wind speeds were defined by Van der Hoven[13] who performed a power spectrum on a time series of wind speeds and identified three distinct peaks of variability: the turbulent peak in the subsecond to minute range, the diurnal peak, and the synoptic peak, which depends on changing weather patterns with a scale of variation that ranges from daily to weekly (Figure 1, with permission from Dutta et al[14]). The annual cycle represents an important peak of variability as well.[15,16]

The overall variability of wind power production, nonetheless, can be diminished by the interconnection between geographically dispersed wind farms[1,4,8,9,12,17-21] since, as distance between wind farms increases, they are affected by distinct weather regimes.[6,22] In this sense, several authors[2,5,18,23] point out that an increased number of turbines within a wind power facility diminish the turbulent variability associated with local features, whereas a wider geographical distribution of wind farms reduces the daily, annual, and synoptic scale variabilities. The latter effect is proportional to the size of the catchment area[1] since the correlation between wind patterns decreases as the distance between sites increases.[21,24]

Argentina has an appreciable potential for wind power generation.[25-27] According to Lu,[27] estimated load factors range between 20% and 50% over the region. Particularly, for the Pampas and Patagonia regions, load factors range between 25% and 50%. Besides the high quality of the wind resource, Argentina has the additional advantage of its wide geographical extension. Its wide latitudinal extension determines the existence of very distinct climatic regimes[28,29]; Patagonia and the Pampas are under the influence of the westerlies while the northern part of the country is under

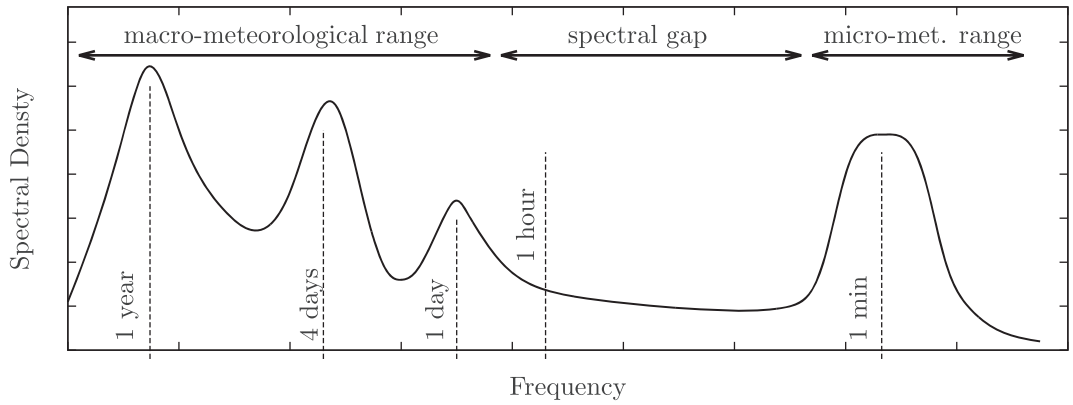

FIGURE 1 Spectral density of wind speeds according to Van der Hoven, adapted from Dutta et al[14]

the influence of the Atlantic anticyclone and the South American low-level jet (SALLJ).[30] For this reason, Argentina might be able to substantially reduce the variability of the wind power output if a planned distribution of wind power facilities makes use of the different wind patterns.

Currently, the country is committed to increase the share of wind generation into its energy matrix. According to the Global Wind Energy Council (GWEC), by the end of 2015, the total wind power installed capacity of Argentina was 279 MW (around 1.3% of the average peak demand).[31] In the last tenders launched by the national government in 2016, 22 projects were awarded for a total of 1472 MW. The purpose of the ongoing tenders is to rise the share of wind energy up to 8% for the year 2018 and up to 20% by the year 2025. At this stage, information about the different spatiotemporal modes of variability of the wind power resource and about the incidence of the geographical dispersion of the projected wind power plants on the overall variability is of great value for decision planners.

The temporal scales defined by Van der Hoven (plus the interannual timescale) can be divided in regular cycles (annual and daily cycles) and irregular cycles (interannual and synoptic scale cycles). At the same time, it is known that geographical variations in the annual and daily wind speed cycles are related to (a) seasonal variations of the semipermanent pressure systems (the semipermanent anticyclones of the Atlantic and Pacific oceans, the Chaco Low) and of the subtropical and polar fronts,[32-34] and to (b) local-scale circulations (related to local surface features and topography[35]). Geographical variations of wind speeds (or wind power production) in the synoptic and interannual timescales are associated with transient weather systems[6,22] and low-frequency climate variations.[36-38] We believe that the separation of wind speeds and wind power production into distinct temporal scales is not arbitrary. The usefulness of this classification lies in the fact that planning and operation activities in a power system are segmented into similar temporal scales, as shown in Parsons et al.[20] Thus, the purpose of this separation is to identify the potential implications for each of those stages of planning and operation. The importance of distinguishing long-term variations from short-term variations lies in that variability of wind speeds on the interannual timescale entails uncertainties related to medium-term (months) strategic planning of the electricity generation mix, whereas variability on the synoptic scale imposes challenges to the operation of the electric grid and might compromise its stability.[20]

The aim of this article is to describe the variability of wind power production over the mentioned timescales over the continental areas of Argentina and Uruguay and to identify the potential implications for the different stages of planning and operation of the power system.

2 | METHODOLOGY

Hourly wind speed data at 50-m height were retrieved from the Modern-Era Reanalysis for Research and Applications 2 (MERRA2, https://gmao.gsfc.nasa.gov/reanalysis/MERRA-2/). Specifically, from the hourly time-averaged single-level diagnostics dataset (tavg1_2d_slv_Nx), MERRA2 and its predecessor MERRA had been widely used to characterize the availability and variability of wind power.[39,40] This dataset was generated using the 5.2.0 version of the Goddard Earth Observing System (GEOS) atmospheric model, together with a data assimilation system. MERRA2 encompasses the 1980 to present period, and its spatial resolution[41] is 0.5° × 0.625°. Grid points over Argentina and Uruguay were extracted, and the regions with elevations above 1500 m.a.s.l. were masked based on the digital elevation model (DEM) ASTER (https://asterweb.jpl.nasa.gov/gdem.asp). The turbulent-scale (or subhourly) variability will not be considered since the temporal resolution of the data used in this study is hourly; and, as mentioned above, the variability over this timescale is filtered by the outputs of the different wind generators within a single wind power facility.[2,5,18,23] Another scale of variability that has important implications in the long-term planning of the power generation system was added to the four described by Van der Hoven: the interannual timescale, that is, the year-to-year fluctuations.

A similar approach as the virtual wind farm (VWF) model developed in Staffell and Green[42] and Staffell and Pfenninger[43] was used to simulate wind power production from wind speeds. For each MERRA grid point, we used 2-, 10-, and 50-m-height hourly wind speeds to compute wind

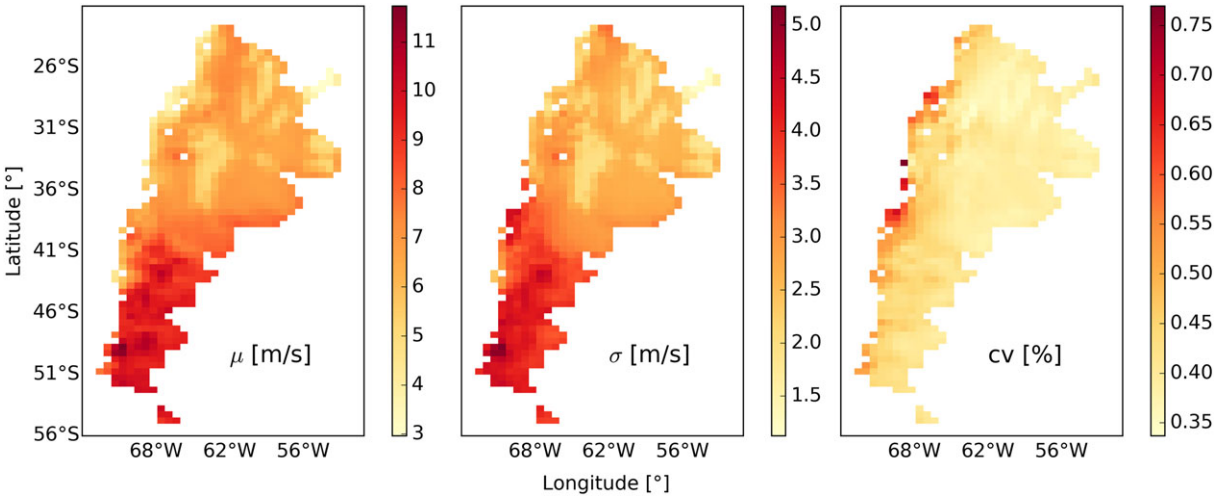

FIGURE 2 Mean wind speeds (left), standard deviation (center), and coefficient of variation (right) [Colour figure can be viewed at wileyonlinelibrary.com]

speeds at 100-m height (the typical hub height of current wind generators) assuming a logarithmic wind profile, by regressing wind speed against the logarithm of height according to the following expression:

$$w(h) = \left(\frac{u*}{k}\right) \log\left(\frac{h-d}{z}\right),$$

where

- h is the height,
- $u*$ is the friction velocity,
- $k = 0.4$ is the Von Karman constant,
- d is the displacement height, and
- z is the surface roughness.

Once data at 100-m height were obtained, wind power outputs were computed using power curves of three International Electrotechnical Commission (IEC) wind classes, according to the mean wind speed at each site. We used three 3.45-MW commercial wind generators power curves:

- Vestas V126 for mean wind speeds below 8 m/s (class IEC IIB-IIIA),
- Vestas V117 for mean wind speeds between 8 and 9.75 m/s (class IEC IB-IIA), and
- Vestas V112 for mean wind speeds above 10 m/s (class IEC-IA).

Before wind speeds with their corresponding power curves are covolved, wind speed values were smoothed using a Gaussian filter, as proposed in the VWF method.

Although MERRA2 is a fair estimation of wind speed time series, it often does not capture local features because of its coarseness. Locally, wind speed is sensible to variations well below its resolution (âĺij 50 km). We compared MERRA2 wind speeds and power simulations with down-scaling simulations using the Weather Research and Forecasting (WRF) model over the existing and projected wind farms (Figure 2). WRF is a state-of-the-art nonhydrostatic high-resolution mesoscale model.[44,45] It was developed (and is regularly updated) by several institutes including the National Center for Environmental Prediction (NCEP) and the National Center for Atmospheric Research (NCAR). The initial and 6-hour boundary conditions were taken from the Global Forecast System (GFS) operational $0.5^\circ \times 0.5^\circ$ resolution global analysis.[46,47] The simulations were performed for a 2-year period from 15 Jan 2015 to 15 Jan 2017. An overview of the model domain configuration and physics schemes used is shown in Table 1.

The frequency domain of the original hourly time series was calculated applying a fast Fourier transform (FFT)[48,49] to the original hourly time series in order to isolate the variability of wind power production over the different timescales proposed by Van der Hoven[13] (daily, synoptic, and annual) plus the interannual timescale:

$$X[k] = \sum_{n=0}^{N-1} x(n) e^{\frac{-j2\pi kn}{N}},$$

where $x(n)$ is the original hourly time series. Then, the resulting spectra ($X(k)$) were filtered using the following ideal rectangular spectral windows: (a) between 0.5 and 2 days for the daily timescale, (b) between 2 and 10 days for the synoptic timescale, (c) between 1 and 13 months for the annual cycle, (d) more than 1 year for the interannual timescale (see Table 2). Finally, the resulting spectra for each case were converted again

TABLE 1 Overview of Weather Research and Forecasting (WRF) configuration

Domain 1 $N_x \times N_y$	40 × 39
Domain 1 grid size	18 km
Domain 2 $N_x \times N_y$	25 × 28
Domain 2 grid size	6 km
N^o of vertical levels	55
Dynamic solver	ARW
period	15 Jan 2015 to 15 Jan 2017
Initial/boundary condition	NCEP GFS analysis (6-h interval)
Microphysics model	Lin et al scheme
Radiation physics	RRTM scheme
Surface-layer physics	Monin-Obukhov (Janjic) scheme
Land-surface physics	Unified Noah LSM
Cumulus physics	Kain-Fritsch (new Eta) scheme
Boundary-layer option	Mellor-Yamada-Janjic TKE scheme

TABLE 2 Timescales involved in the analysis

Timescale	Period τ
Daily	0.5 d < τ < 2 d
Synoptic	2 d < τ < 10 d
Annual	1 mo < τ < 13 mo
Interannual	τ > 1 y

into the time domain using an inverse Fourier transform:

$$x_i(n) = \sum_{k=0}^{N-1} (X(k) * W(k)) e^{\frac{j2\pi kn}{N}},$$

where $W(k)$ is the corresponding rectangular spectral window.

The Van der Hoven spectrum (Figure 1) has been the reference wind speed spectrum in wind engineering since its publication in 1957.[14,50,51] The practicality of the Van der Hoven spectrum lies in that it revealed a spectral gap (centered approximately on a frequency of 1 cycle/h), which divides the macrometeorological (synoptic and daily) from micrometeorological fluctuations.[52-54] The representativeness of the Van der Hoven Spectrum has been questioned in recent years mainly because of the fact that it was calculated using limited computing capabilities and that wind speeds were recorded at unusually gusty conditions (during the passage of a hurricane).[55,56] Despite this, different wind speed spectrums calculated at diverse conditions seem to capture the overall shape proposed by Van der Hoven.[53-56] It is likely that variables such as the location, height, resolution, and period of time at which a wind speed spectrum is calculated determine the proportion of variance explained by the different spectral peaks. This study is not aimed to quantify the importance of each timescale (that should be matter of further investigations). We will use the timescales proposed by Van der Hoven as a reference by which to analyze the effect of wind speed variability in the operation and planning activities of a power system.

In this study, we aim to analyze the spatiotemporal variability of potential wind power production within the entire territory of Argentina and Uruguay. This implies a very large number of time series (for instance, each MERRA2 grid node) to be included in the analysis. It is not desirable nor practical to analyze each time series separately, so it is then necessary to implement a statistical method that synthesizes the information of the wind power production fields for each timescale analyzed. In climate studies, the empirical orthogonal function (EOF) analysis is commonly used to study possible spatial structures of variability and how they change with time.[57,58] This method reprojects data matrices onto orthogonal axes called EOFs that capture the main modes of variability.[59,60] Specifically, this method first transforms the original data matrix A_{orig} into a zero mean vector by subtracting the mean value to each corresponding row of A_{orig}, that is, $A = A_{orig} - \bar{a} * I$, where I is the column vector of all ones, while $\bar{a}$ is the vector of sample means. Then, the covariance matrix is computed as $S = \frac{1}{n-1} A * A^T$. Finally, the eigenvectors v and the eigenvalues λ are computed from the covariance matrix: $Sv = \lambda v$.

It is demonstrated in Hannachi et al[61] and Navarra and Simoncini[60] that the number of independent maps (or vectors) in the original datasets is the same as the orthogonal set of eigenvectors of the covariance matrix and that the variance explained by each eigenvector is proportional to the eigenvalues.

A somehow similar approach was used by Mahecha et al[62] to study the spatiotemporal modes of variability of a Fraction of a Absorbed Photosynthetically Active Radiation (FAPAR) dataset. They applied the singular system analysis (SSA) to decompose the original time series into

TABLE 3 Comparison between MERRA2 and WRF-derived wind speeds at 100-m height and wind power production at existing and projected wind farms

			$\bar{v}_{h=100m}$ (m/s)		Correlation	Weibull *k*		CF	
ID	lat	lon	MERRA	WRF	MERRA-WRF	MERRA	WRF	MERRA	WRF
1	−34.84	−69.33	5.04	8.49	0.61	1.77	1.68	0.19	0.36
2	−28.75	−66.75	3.98	7.36	0.37	2.01	2.00	0.09	0.41
3	−29.42	−63.71	6.56	9.91	0.63	3.98	2.70	0.28	0.55
4	−33.14	−64.96	5.79	8.64	0.41	3.11	2.20	0.22	0.46
5	−34.20	−62.90	5.72	9.08	0.48	3.46	1.80	0.20	0.48
6	−37.10	−57.80	7.16	8.80	0.70	3.29	2.45	0.36	0.50
7	−38.27	−57.83	8.29	9.82	0.78	2.63	2.24	0.45	0.55
8	−38.56	−58.75	7.92	9.33	0.77	2.84	2.28	0.46	0.51
9	−36.64	−60.34	6.83	8.59	0.68	3.09	2.43	0.33	0.49
10	−37.43	−64.72	6.65	8.86	0.68	3.08	2.23	0.31	0.50
11	−38.82	−60.32	7.75	9.62	0.75	3.06	2.31	0.44	0.54
12	−38.61	−62.34	7.84	9.36	0.73	3.02	2.19	0.45	0.51
13	−38.71	−62.53	7.87	9.07	0.72	3.02	2.31	0.45	0.51
14	−38.36	−62.21	7.87	9.69	0.73	3.02	2.24	0.45	0.54
15	−38.24	−62.32	8.11	9.49	0.73	3.01	2.28	0.43	0.53
16	−38.62	−62.02	8.11	9.38	0.75	3.01	2.36	0.43	0.52
17	−38.67	−61.96	8.11	9.31	0.75	3.01	2.34	0.43	0.52
18	−38.82	−62.70	7.72	9.03	0.70	3.15	2.51	0.43	0.53
19	−39.25	−62.62	7.82	9.28	0.68	3.27	2.52	0.44	0.52
20	−40.03	−62.66	7.93	9.55	0.71	3.18	2.57	0.45	0.54
21	−40.55	−63.02	8.14	9.52	0.70	2.91	2.40	0.44	0.53
22	−40.80	−63.87	8.14	10.12	0.74	2.79	2.34	0.44	0.57
23	−40.80	−65.20	7.74	9.67	0.68	2.48	2.34	0.44	0.55
24	−39.35	−65.59	7.50	8.93	0.68	2.88	2.20	0.41	0.51
25	−43.12	−65.26	8.58	9.97	0.73	2.68	2.23	0.48	0.56
26	−42.64	−65.26	8.58	9.84	0.71	2.68	2.36	0.48	0.56
27	−43.35	−65.18	8.47	9.96	0.77	2.46	2.44	0.47	0.56
28	−42.38	−69.28	9.73	9.38	0.82	2.45	2.16	0.53	0.51
29	−44.71	−66.73	8.97	10.72	0.76	2.89	2.45	0.50	0.61
30	−44.92	−66.99	9.30	11.29	0.78	2.77	2.47	0.51	0.65
31	−45.67	−67.81	9.88	12.40	0.81	2.58	2.35	0.55	0.69
32	−45.85	−67.50	9.54	11.79	0.79	2.35	1.85	0.52	0.60
33	−45.78	−67.67	9.54	12.98	0.79	2.35	1.97	0.52	0.65
34	−45.79	−68.06	9.58	11.73	0.81	2.49	2.48	0.53	0.67
35	−46.70	−68.40	9.13	10.61	0.79	2.52	2.05	0.51	0.59
36	−46.55	−68.95	9.05	10.82	0.81	2.45	2.13	0.50	0.61
37	−46.82	−67.94	8.62	10.97	0.73	2.68	2.28	0.47	0.62
38	−47.18	−67.14	8.89	10.46	0.70	2.76	2.36	0.50	0.60
39	−47.55	−66.18	9.06	10.57	0.71	2.94	2.36	0.52	0.61
40	−49.93	−68.85	9.02	9.48	0.77	2.56	2.05	0.51	0.51
41	−40.73	−70.58	6.70	8.42	0.71	2.13	2.32	0.32	0.46
42	−38.86	−70.05	7.24	8.27	0.75	2.18	1.69	0.36	0.39
43	−39.83	−68.63	7.94	7.97	0.62	2.56	1.82	0.44	0.45
44	−38.93	−68.56	7.05	7.86	0.73	2.12	1.80	0.37	0.45
45	−38.87	−68.23	7.41	8.30	0.74	2.37	1.83	0.40	0.46
46	−39.36	−69.04	7.48	8.10	0.71	2.23	1.69	0.41	0.44

Abbreviations: MERRA, Modern-Era Retrospective Analysis for Research and Applications; WRF, Weather Research and Forecasting.

low frequency, annual/seasonal, and high-frequency modes and then applied classical multidimensional scaling (CMDS) to obtain the main modes of geographical variability associated with each timescale.

We included Uruguay in this study since both countries trade electricity on a regular basis. Both countries are interconnected by two 500-kV power lines (http://portalweb.cammesa.com/Descargas archivos/GEOSADI2017_04.pdf), and they jointly operate the run-of-river Salto Grande hydropower plant (1890 MW).

3 | RESULTS

Table 3 shows the comparisons between MERRA2 and WRF wind speeds and power simulations. In all cases, the mean wind velocities and capacity factors simulated with WRF are higher. We also computed the Weibull *k* factor for both MERRA2 and WRF hourly data. WRF shows lower *k* values, indicating a higher dispersion of velocity values. Nevertheless, MERRA2 and WRF simulations show, in most of the sites, significant correlation coefficients.

A preliminary analysis of the wind speed and wind power production estimations confirms that the region has a high-quality wind resource. Figure 2 shows the average wind speeds, standard deviation, and coefficient of variation at 100-m height. The windiest region is, by far, Patagonia, where wind speeds range between 8 and 12 m/s. Wind speeds range between 6 and 9 in central Argentina and above 5 m/s in most northern Argentina and Uruguay. The windiest regions broadly coincide with the highest average annual capacity factors (Figure 3). Capacity factors range between approximately 0.5 and 0.6 in Patagonia (south of 40° S), between 0.4 and 0.55 in central Argentina (between 36° and 43° S), and above 0.3 in most northern Argentina and Uruguay.

It can be seen in Figure 3E that most projected and existing wind farms have prioritized high wind speeds and capacity factors. Although this variable is a determinant to define the economic feasibility of a single facility, it does not completely describe the variability of the whole of the wind resource nor provide a tool for an adequate planning in which different wind regimes can be compensated. Patagonia, for example, despite having high-average wind speeds and capacity factors, also shows high standard deviations in wind speeds (above 3 m/s and up to 5 m/s, Figure 3). This characteristic could be problematic when integrating wind farms into the national grid. In terms of intermittency, the grid administrator, for instance, has to deal with the absolute variations in meter per second and megawatt. In the following sections, we will analyze the overall wind energy production over different timescales: interannual, annual, synoptic, and daily.

3.1 | Interannual variability

The EOF analysis performed on the time series of wind power outputs in which the interannual variability has been isolated allowed the identification of three significant spatiotemporal patterns of variability (Figure 4). The percentage of variability explained by each pattern (or EOF) is indicated in the corresponding panel. The first EOF is most intensely expressed over Patagonia; the second EOF indicates the existence of a dipole (opposite temporal behavior) between northwestern and southern Patagonia; and the third EOF is associated with wind variations over central Argentina (with higher loads over northern Patagonia).

The resulting EOFs show differentiated temporal behaviors (Figure 5); in the EOF 1, the 1.3- and the 15-year cycles and the cycles contained in the 2- to 3-year spectral window stand out. In the EOF 2, the most prominent cycles are centered approximately at 10 and 3 years, while 5- and 2.5-year cycles stand out in EOF 3.

Correlation maps between each EOF time series and sea-level pressures (SLPs) derived from MERRA2 were calculated in order to identify the circulation features associated with each wind variability pattern (Figure 6). The results indicate that each EOF is associated with a known

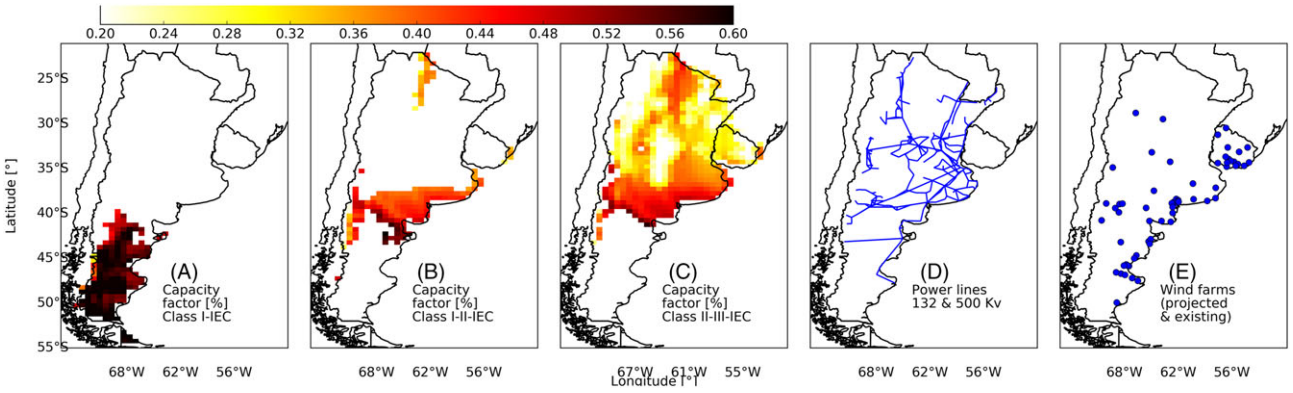

FIGURE 3 Average annual capacity factors of the International Electrical Comission (IEC) wind class A, I, B, I-II, and C, II-III, D, power transmission lines of Argentina (>132 kV), and E, projected and existing wind farms [Colour figure can be viewed at wileyonlinelibrary.com]

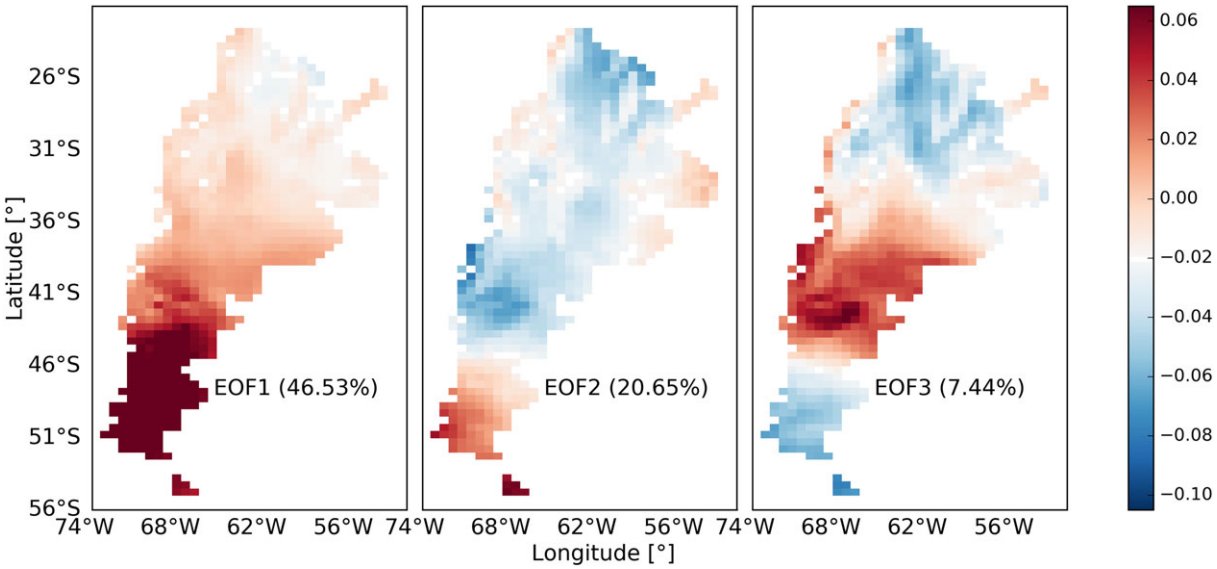

FIGURE 4 The three leading empirical orthogonal functions (EOFs) of filtered hourly wind speeds (interannual variability). The variance explained by each spatial pattern is indicated in the figure [Colour figure can be viewed at wileyonlinelibrary.com]

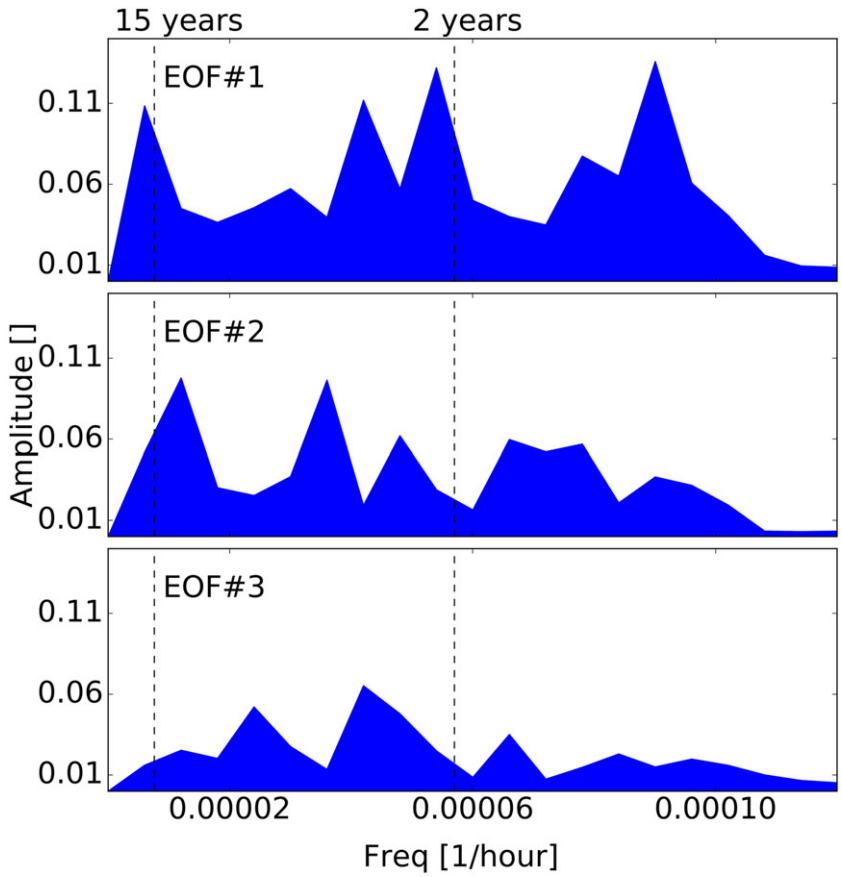

FIGURE 5 Power spectrum of the time series of the empirical orthogonal functions (EOFs) 1, 2, and 3 applied on the filtered hourly wind speeds (interannual scale) [Colour figure can be viewed at wileyonlinelibrary.com]

mode of variability of the atmospheric circulation. EOF 1 is related to pressure anomalies of opposite sign between (a) the subtropical Pacific ocean and (b) the south of 50°, including the southern tip of the continent, the Drake passage, and the southern Atlantic ocean. Weak winds over Patagonia are associated with anticyclonic anomalies over the southern Atlantic ocean, and vice versa. Garreaud et al[63] point out that anticyclonic anomalies over Patagonia (and thus eastward wind anomalies) are negatively correlated with precipitation over the Cordillera de los

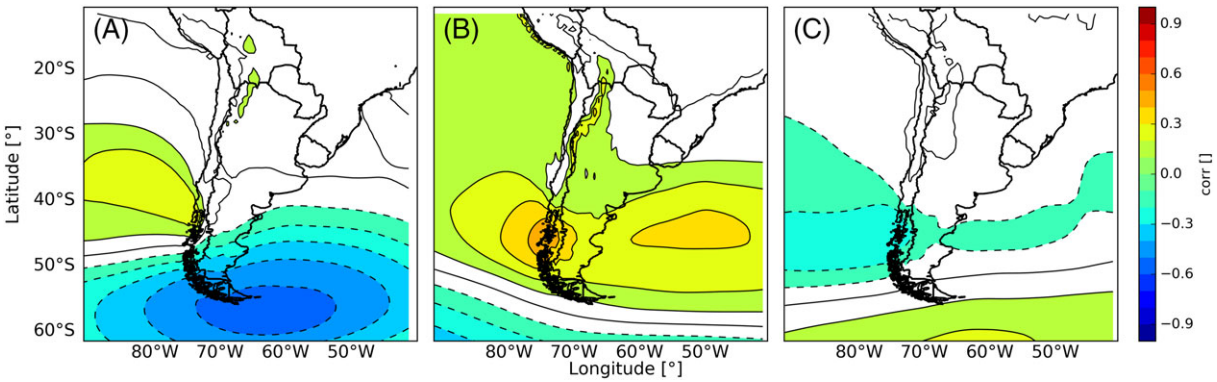

FIGURE 6 Correlation maps between the principal components of the empirical orthogonal functions (EOFs) A, 1, B, 2, and C, 3 and sea-level pressure (SLP). Significant correlations at the 99% confidence level are colored [Colour figure can be viewed at wileyonlinelibrary.com]

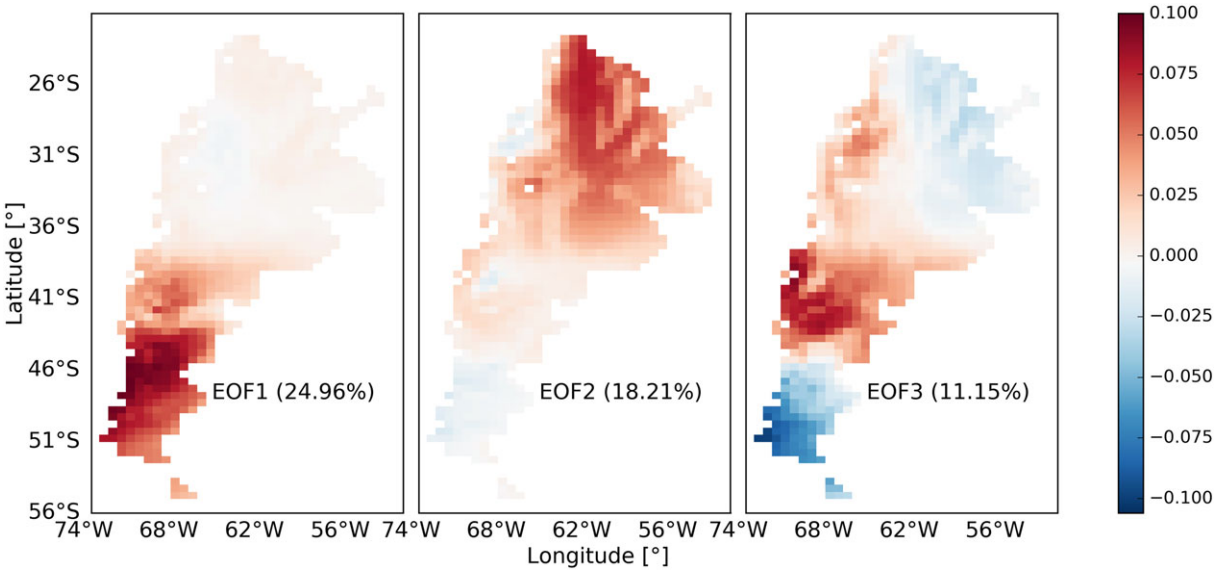

FIGURE 7 The three leading empirical orthogonal functions (EOFs) of filtered hourly wind speeds (annual variability). The variance explained by each spatial pattern is indicated in the figure [Colour figure can be viewed at wileyonlinelibrary.com]

Andes (and vice versa; cyclonic anomalies over Patagonia are positively correlated with precipitation over the Cordillera de los Andes).

The EOFs 2 and 3 are related to pressure anomalies of opposite sign between southern Argentina (Patagonia) and subpolar latitudes (south of 55° S approximately). Hence, positive wind power production anomalies over southern Patagonia (middle pannel in Figure 4) are associated with positive SLP anomalies over that region (middle pannel in Figure 6) and strong latitudinal pressure gradient, while positive wind power production anomalies over central Argentina and Northern Patagonia (right pannel in Figure 4) are associated with low-pressure anomalies over the 40° to 50° latitudinal band.

3.2 | Annual variability

The EOF analysis performed on the time series in which the annual cycle has been isolated allowed the identification of diverse spatiotemporal variability patterns. The first EOF (left side panel of Figure 7) expresses the variability of wind speeds over Patagonia. The reason why this region explains the largest portion of variance is related to the fact that Patagonia is, by far, the windiest region and the standard deviations of wind speeds seem to be larger where the mean values are larger (Figure 2). The annual cycle that is immersed in this EOF shows, on average, minimum values during late summer and early fall and during spring and maximum values during late spring/early summer. It also shows a secondary maximum during late fall (Figure 8).

The second EOF expresses the variability over northern Argentina, with higher loads over the Chaco region. The temporal behavior of this EOF is dominated by a strong annual cycle, which shows two maximums during early fall and spring and minimums during summer and winter.

The third EOF (right panel of Figure 7) shows a dipole pattern between two regions (southward and northward of approximately 46° S, southern and northern Patagonia, respectively) with opposite temporal behaviors. The average annual cycle of this EOF shows maximum (minimum) values

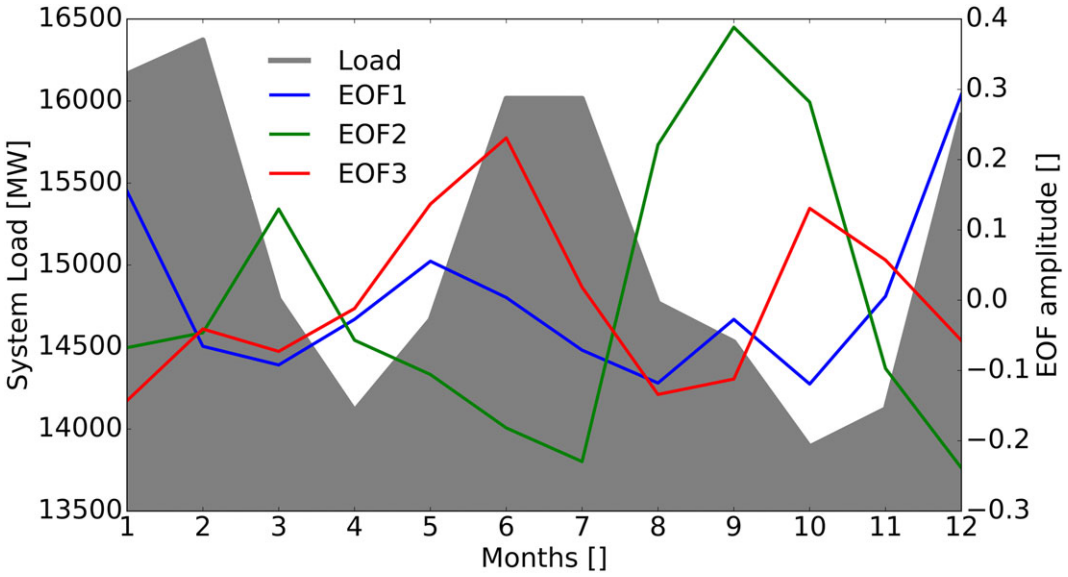

FIGURE 8 Annual averages of the principal components of empirical orthogonal functions (EOFs) 1, 2, and 3 and the average annual electricity load (source: Compañía Administradora del Mercado Mayorista Eléctrico Argentino) [Colour figure can be viewed at wileyonlinelibrary.com]

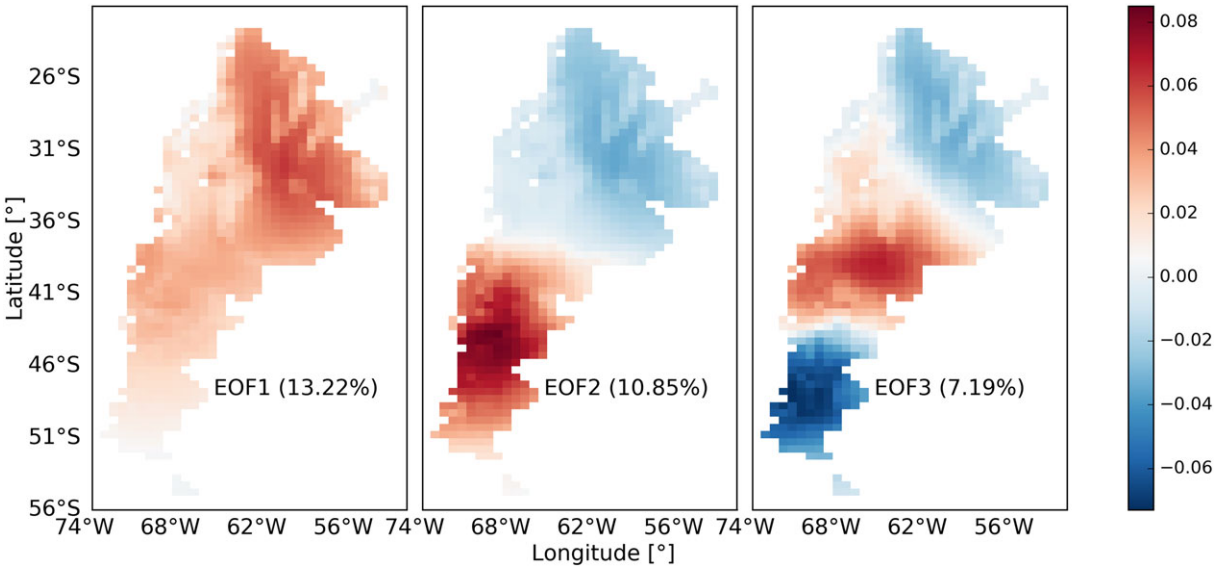

FIGURE 9 The three leading empirical orthogonal functions (EOFs) of filtered hourly wind speeds (synoptic scale variability). The variance explained by each spatial pattern is indicated in the figure [Colour figure can be viewed at wileyonlinelibrary.com]

during late fall and early winter and during spring and minimum (maximum) values during summer and late winter over northern (southern) Patagonia. It is worth mentioning the complementarity between the annual averages of the different EOFs shown in Figure 8. The average annual load curve shows two seasonal maxima, during summer and winter, and two seasonal minima, during autumn and spring, while potential wind power production speed peak during summer over Patagonia (EOF 1) and during winter over northern Patagonia (EOF 3).

3.3 | Synoptic variability

The EOF analysis applied to the time series in which the synoptic scale variability has been isolated identifies three dominant variability patterns (Figure 9). The first EOF is expressed over a large region that includes central and northern Argentina plus Uruguay. The second EOF represents the variability over central Patagonia. The harmonics included between (approximately) the 26 to 13 days, the 8- to 4-day spectral gaps, and the 3- and 2-day harmonics stand out. The second EOF shows a dipole (opposite behavior) between Patagonia (south of 44° S) and the rest of the study area. Patagonia, as in the other timescales analyzed, shows a higher variability than the other EOFs (Figure 10) because of the higher standard deviation of wind speeds over this region (Figure 2). The harmonics included in the 26 to 4 days contribute with the highest percentage of explained variance, with maxima at approximately 20, 17, and 8 days. There are also local variability maxima at the ~ 2.5-day harmonics.

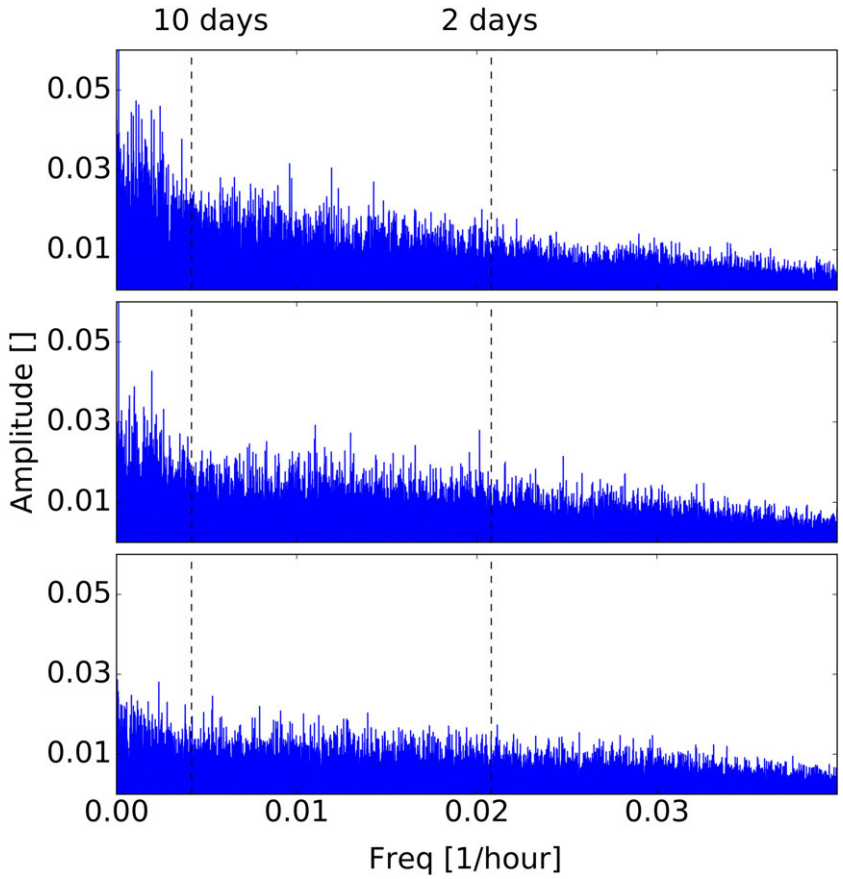

FIGURE 10 Power spectrum of the principal components of the empirical orthogonal functions (EOFs) 1, 2, and 3 applied on the filtered hourly wind speeds (synoptic scale) [Colour figure can be viewed at wileyonlinelibrary.com]

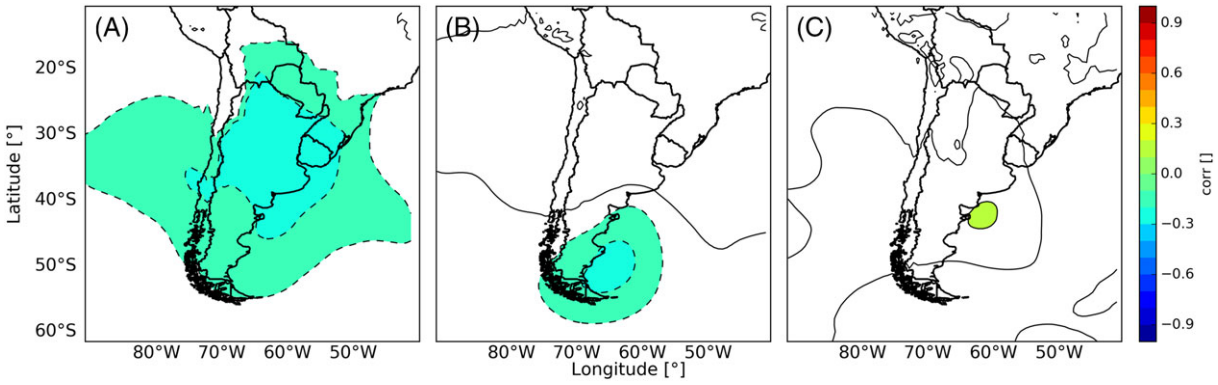

FIGURE 11 Correlation maps between time series of the empirical orthogonal functions (EOFs) A, 1, B, 2, and C, 3 and sea-level pressure (SLP). Significant correlations at the 99% confidence level are colored [Colour figure can be viewed at wileyonlinelibrary.com]

The third EOF shows opposing behaviors between southern Patagonia (south of 46°) plus northeastern Argentina plus Uruguay and northern Patagonia. All three EOFs show a "red noise" spectrum (Figure 10) with a higher contribution of low-frequency cycles (periods >10 d).

As with the interannual analysis, correlations between the time series of each EOF and the SLPs were computed (Figure 11) in order to identify the atmospheric circulation configurations associated with each mode of variability. Each EOF is associated with known and distinct circulation features. EOF 1 is negatively associated with SLP variations over a large area, which includes Argentina, Chile, Paraguay, Uruguay, and southern Brazil. This mode resembles the shape of the typical anticyclone that enters the continent from the Pacific Ocean across the lowest portion of the Andes. The incursions of such anticyclones occur all year round with a periodicity of around 2 weeks.[64-66] The incursions of such anticyclones into the continent cause weak winds over the region. EOF 2 is negatively associated with pressure anomalies over southeast Patagonia. These anomalies are, thus, related to the passage of transient high- and low-pressure systems with west-eastward or southwest-northeastward trajectories and strongly modulate the weather over south central Argentina and Uruguay.[29,66] The sign of the correlations implies that higher (lower) wind speeds are associated with negative (positive) pressure anomalies.

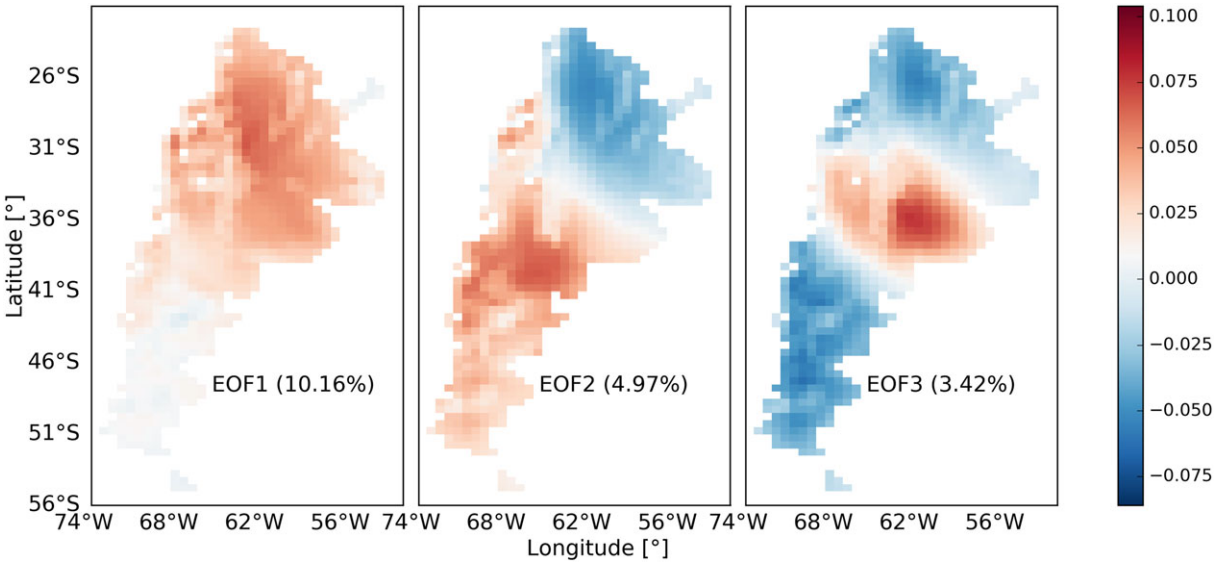

FIGURE 12 The three leading empirical orthogonal functions (EOFs) of filtered hourly wind speeds (daily variability). The variance explained by each spatial pattern is indicated in the figure [Colour figure can be viewed at wileyonlinelibrary.com]

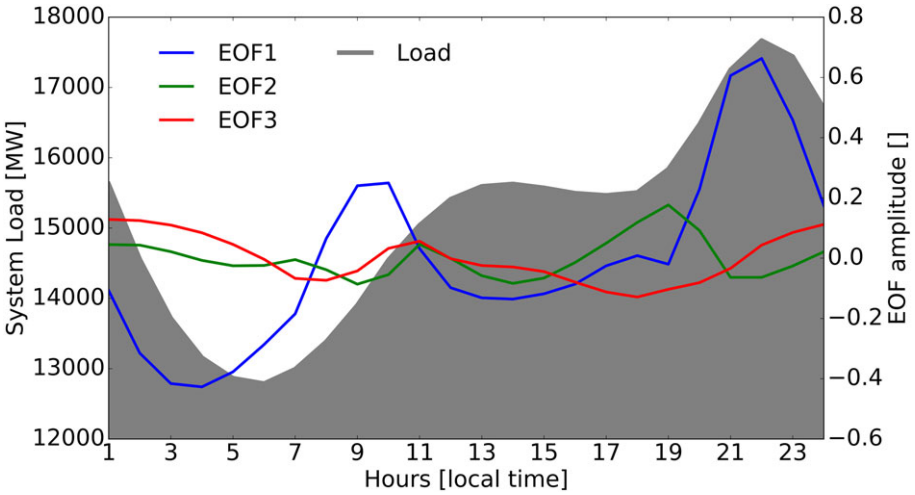

FIGURE 13 Daily averages of the principal components of empirical orthogonal functions (EOFs) 1, 2, and 3 and the average daily electricity load (source: Compañía Administradora del Mercado Mayorista Eléctrico Argentino) [Colour figure can be viewed at wileyonlinelibrary.com]

3.4 | Daily variability

The EOF analysis performed on the time series in which the daily cycle has been isolated identifies three spatiotemporal variability patterns. The first EOF (Figure 12) represents the variability over central and northern Argentina plus Uruguay; and it is associated with an average daily cycle, which shows a maximum at around 22:00 (local time), a minimum between 04:00 and 06:00, and a secondary maximum around 10:00 (Figure 13). The average daily cycles of the first EOF follow the average daily electric load closer than the remaining EOFs. The second EOF indicates an opposing behavior between central Argentina and northeastern Argentina plus Uruguay. The diurnal cycle associated with this EOF shows rather constant values throughout the day, reaching a maximum at around 19:00. It should be mentioned, nevertheless, that the overall variance explained by these EOFs is low (less than 20%) so the implication of these results should be taken carefully.

The third EOF indicates opposing temporal behaviors between central Argentina and northern Argentina and Patagonia. The temporal behavior associated with this EOF shows, on average, rather constant wind speeds throughout the day. Values are higher, on average, between 21:00 and 06:00 and lower from 08:00 on (Figure 13).

4 | DISCUSSION AND CONCLUSIONS

The temporal behavior of wind speeds (and hence wind power production) is spatially heterogeneous, and this heterogeneity varies according to which timescale is analyzed. On the annual timescale (monthly time series), we found that (a) wind power potential peaks, on average, during

summer over Patagonia, during fall over Patagonia and northern Argentina plus Uruguay, during winter over northern Patagonia and central Argentina, and during spring over central and northern Argentina plus Uruguay. The EOF performed on the filtered hourly time series in which the daily cycle has been isolated identifies three significant variability patterns. EOF 1 shows a well-defined daily cycle, which follows the daily average load curve closer than EOFs 2 and 3.

As from the EOF analysis applied to the synoptic filtered hourly time series, we conclude that (a) the passage of transient pressure systems over central Argentina and Patagonia is the main source of variability of wind power production in the synoptic scale and (b) there are two patterns of opposite temporal behavior (a) between Patagonia and the rest of the study area and (b) between southern Patagonia plus northwest Argentina plus Uruguay and northern Patagonia. These patterns are associated with distinct atmospheric circulation features, the passage of the typical mid-latitude transient low- and high-pressure systems.

On the interannual timescale, the variability patterns are associated, in general, with dipoles of pressure anomalies. This implies the simultaneous occurrence of negative wind speed anomalies in a certain region together with positive anomalies in another region. In this sense, on the interannual timescale, southern Patagonia and northern Patagonia (EOF 2) show an opposite behavior, whereas northern Argentina plus southern Patagonia and central Argentina show an opposite behavior (EOF 3).

These dipole pressure correlation patterns between mid and high latitudes might have implications in the future performance of wind farms in the region because of projected climate trends. Several authors have reported a positive trend in surface pressures over the southern hemisphere mid latitudes since the mid[67-71] that would imply weaker wind speeds over northern Patagonia and central Argentina.[38] There are many articles that suggest that the observed changes might have been driven by changes in the circulation of the polar vortex because of the ozone depletion, which in turn affect the position of the mid-latitude jet and the width of the Hadley cell.[72-83] Other studies suggest that these positive trends coincide with the response pattern of the southern hemisphere changes in the atmospheric circulation due to global warming, which implies a poleward shift of the mid-latitude jet.[76,77,84-87] Thus, over the next decades, the recovery of the ozone hole and the increase of anthropogenic warming are expected to exert opposite effects upon the pressure distribution over the southern hemisphere. Which of those forcings will dominate is still a matter of debate.[81,82]

The heterogeneous characteristic of the wind regimes has important implications for the generation of wind energy. For example, even though that wind farms deployed in Patagonia would introduce interannual and synoptic scale "noise," the combination with wind farms deployed in northern Patagonia and central Argentina would result in an output that follows the annual load curve, since wind power production in Patagonia peaks during summer and autumn, while it peaks during winter in northern Patagonia and central Argentina.

Moreover, the average daily output of wind farms deployed in northern Argentina would follow the average daily load curve closer than the other regions. The importance of this result lies in that (a) power produced by an intermittent source during peak-load periods is worth more than the power produced during the minimum-load periods[88] and (b) few wind parks had been projected in this region. Patagonia, central Argentina, and Uruguay are preferred locations because of the quality of the resource and their closeness to the consumption areas and power transmission lines (Figure 3E).

The results of the EOF analysis performed over the different timescales affirm the importance of geographical distribution of the wind energy production. When planning the introduction of wind generation into an electricity generation mix, it is important to consider not only the mean wind speeds, capacity actors, or the availability of the grid to transport the production but also the complementarity between different regions in order to (a) diminish the random variability and (b) produce, if possible, more wind power during the peak-demand months and hours.

ACKNOWLEDGEMENTS

The authors would like to thank Jorge Siryi and Joaquin Beitia of the Compañía Administradora del Mercado Mayorista Eléctrico de Argentina (CAMMESA) who encouraged this research and provided load data. This work was supported by (a) Agencia Nacional de Promoción Científica y Tecnológica and (b) Universidad Nacional de Río Negro.

ORCID

Emilio Bianchi https://orcid.org/0000-0003-1300-2198

REFERENCES

1. Archer CL, Jacobson MZ. Supplying baseload power and reducing transmission requirements by interconnecting wind farms. *J Appl Meteorol Climatol*. 2007;46(11):1701-1717.
2. Sovacool BK. The intermittency of wind, solar, and renewable electricity generators: technical barrier or rhetorical excuse? *Util Policy*. 2009;17(3):288-296.
3. Suberu MY, Mustafa MW, Bashir N. Energy storage systems for renewable energy power sector integration and mitigation of intermittency. *Renew Sustain Energy Rev*. 2014;35:499-514.
4. Kahn E. The reliability of distributed wind generators. *Electr Pow Syst Res*. 1979;2(1):1-14.
5. DeMeo EA, Grant W, Milligan MR, Schuerger MJ. Wind plant integration [wind power plants]. *IEEE Power Energ Mag*. 2005;3(6):38-46.

6. Grams CM, Beerli R, Pfenninger S, Staffell I, Wernli H. Balancing Europe's wind-power output through spatial deployment informed by weather regimes. *Nat Clim Change*. 2017;7(8):557.
7. Piwko R, Osborn D, Gramlich R, Jordan G, Hawkins D, Porter K. Wind energy delivery issues [transmission planning and competitive electricity market operation]. *IEEE Power Energ Mag*. 2005;3(6):47-56.
8. Gross R, Heptonstall P, Leach M, Skea J, Anderson D, Green T. The UK Energy Research Centre review of the costs and impacts of intermittency. *Renewable Electr Grid Chall Var*. 2012:73.
9. Cosseron A, Gunturu UB, Schlosser CA. Characterization of the wind power resource in Europe and its intermittency. *Energy Procedia*. 2013;40:58-66.
10. Milligan M, Porter K. Determining the capacity value of wind: a survey of methods and implementation. NREL/CP-500-38062, Golden, CO (US), National Renewable Energy Lab.; 2005.
11. Albadi MH, El-Saadany EF. Overview of wind power intermittency impacts on power systems. *Electr Pow Syst Res*. 2010;80(6):627-632.
12. Fant C, Gunturu B, Schlosser A. Characterizing wind power resource reliability in southern Africa. *Appl Energy*. 2016;161:565-573.
13. Van der Hoven I. Power spectrum of horizontal wind speed in the frequency range from 0.0007 to 900 cycles per hour. *J Meteorol*. 1957;14(2):160-164.
14. Dutta R, Wang F, Bohlmann BF, Stelson KA. Analysis of short-term energy storage for midsize hydrostatic wind turbine. *J Dyn Syst Meas Control*. 2014;136(1):011007.
15. Wieringa J. Shapes of annual frequency distributions of wind speed observed on high meteorological masts. *Boundary Layer Studies and Applications*: Springer; 1989:85-110.
16. Isyumov N. Alan G. Davenport's mark on wind engineering. *J Wind Eng Ind Aerodyn*. 2012;104:12-24.
17. Milligan MR, Artig R. Reliability benefits of dispersed wind resource development. NREL/CP-500-24314; CONF-980437-, Golden, CO (US), National Renewable Energy Laboratory; 1998.
18. Milligan MR, Artig R. Choosing wind power plant locations and sizes based on electric reliability measures using multiple-year wind speed measurements. NREL/CP-500-26724, Golden, CO (US), National Renewable Energy Lab.; 1999.
19. Simonsen TK, Stevens BG. Regional wind energy analysis for the central United States. *Proc Global Wind Power*. 2004:16.
20. Parsons BK, Milligan M, Smith JC, et al. Grid impacts of wind power variability: recent assessments from a variety of utilities in the United States. NREL/CP-500-39955, Golden, CO (United States), National Renewable Energy Laboratory; 2006.
21. Sinden G. Characteristics of the UK wind resource: long-term patterns and relationship to electricity demand. *Energy Policy*. 2007;35(1):112-127.
22. Bett PE, Thornton HE. The climatological relationships between wind and solar energy supply in Britain. *Renew Energy*. 2016;87:96-110.
23. Ackermann T. *Wind Power in Power Systems*. Chichester: John Wiley & Sons; 2005.
24. Wan Y-H. Wind power plant behaviors: analyses of long-term wind power data. NREL/CP-500-36551, Golden, CO (US), National Renewable Energy Lab.; 2004.
25. Hoogwijk M, de Vries B, Turkenburg W. Assessment of the global and regional geographical, technical and economic potential of onshore wind energy. *Energy Econ*. 2004;26(5):889-919.
26. De Vries BJM, Van Vuuren DP, Hoogwijk MM. Renewable energy sources: their global potential for the first-half of the 21st century at a global level: an integrated approach. *Energy Policy*. 2007;35(4):2590-2610.
27. Lu X, McElroy MB, Kiviluoma J. Global potential for wind-generated electricity. *Proc Natl Acad Sci*. 2009;106(27):10933-10938.
28. Prohaska F. The climate of Argentina, Paraguay and Uruguay. *Climates Cent South Amer*. 1976;12:13-112.
29. Garreaud RD, Vuille M, Compagnucci R, Marengo J. Present-day south American climate. *Palaeogeogr Palaeoclimatol Palaeoecol*. 2009;281(3):180-195.
30. Marengo JA, Soares WR, Saulo C, Nicolini M. Climatology of the low-level jet east of the Andes as derived from the NCEP–NCAR reanalyses: characteristics and temporal variability. *J Clim*. 2004;17(12):2261-2280.
31. Renewables REN21. Global status report. Renewable Energy Policy Network for the 21st Century; 2016.
32. Rao VB, Do Carmo AMC, Franchito SH. Seasonal variations in the southern hemisphere storm tracks and associated wave propagation. *J Atmos Sci*. 2002;59(6):1029-1040.
33. Nakamura H, Shimpo A. Seasonal variations in the southern hemisphere storm tracks and jet streams as revealed in a reanalysis dataset. *J Clim*. 2004;17(9):1828-1844.
34. Saulo AC, Ferreira LJ, Mejia J, Seluchi M. Description of the thermal low characteristics using SALLJEX special observations. *Clivar Exch*. 2004;9(1):9-10.
35. Oke TR. *Boundary Layer Climates*. London & New York: Routledge; 2002.
36. Harper BR, Katz RW, Harriss RC. Statistical methods for quantifying the effect of the El Niño—southern oscillation on wind power in the northern great plains of the United States. *Wind Eng*. 2007;31(3):123-137.
37. Torres Silva dos Santos A, e Silva S, Moisés C. Seasonality, interannual variability, and linear tendency of wind speeds in the northeast Brazil from 1986 to 2011. *Sci World J*. 2013;2013.
38. Bianchi E, Solarte A, Guozden TM. Large scale climate drivers for wind resource in southern South America. *Renew Energy*. 2017;114:708-715.
39. Cannon DJ, Brayshaw DJ, Methven J, Coker PJ, Lenaghan D. Using reanalysis data to quantify extreme wind power generation statistics: a 33 year case study in Great Britain. *Renew Energy*. 2015;75:767-778.
40. Olauson J, Bergkvist M. Modelling the Swedish wind power production using MERRA reanalysis data. *Renew Energy*. 2015;76:717-725.
41. Rienecker MM, Suarez MJ, Gelaro R, et al. MERRA: NASA's Modern-Era Retrospective Analysis for Research and Applications. *J Clim*. 2011;24(14):3624-3648.
42. Staffell I, Green R. How does wind farm performance decline with age? *Renew Energy*. 2014;66:775-786.
43. Staffell I, Pfenninger S. Using bias-corrected reanalysis to simulate current and future wind power output. *Energy*. 2016;114:1224-1239.
44. Skamarock WC, Klemp JB, Dudhia J, et al. A description of the advanced research WRF version 2. NCAR/TN-468+ STR, National Center For Atmospheric Research Boulder Co Mesoscale and Microscale Meteorology Div; 2005.
45. Skamarock WC, Klemp JB. A time-split nonhydrostatic atmospheric model for weather research and forecasting applications. *J Comput Phys*. 2008;227(7):3465-3485.

46. Campana K, Caplan P, Alpert J. Technical procedures bulletin for the T382 Global Forecast System; 2005.
47. Saha S, Moorthi S, Wu X, et al. The NCEP climate forecast system version 2. *J Clim*. 2014;27(6):2185-2208.
48. von Storch H, Zwiers FW. Statistical analysis in climate research; 2002.
49. Bloomfield P. *Fourier Analysis of Time Series: An Introduction*. New York: John Wiley & Sons; 2004.
50. Burton T, Sharpe D, Jenkins N, Bossanyi E. *Wind Energy Handbook*. New York: John Wiley & Sons; 2001.
51. Neammanee B, Sirisumrannukul S, Chatratana S. Development of a wind turbine simulator for wind generator testing. *Int Energy J*. 2007;8(1).
52. Böttcher F, Peinke J. Small and large scale fluctuations in atmospheric wind speeds. *Stochastic Environ Res Risk Assess*. 2007;21(3):299-308.
53. Harris RI. The macrometeorological spectrum—a preliminary study. *J Wind Eng Ind Aerodyn*. 2008;96(12):2294-2307.
54. Kaya E, Barutcu B, Menteş ŞS. A method based on the Van der Hoven spectrum for performance evaluation in prediction of wind speed. *Turk J Earth Sci*. 2013;22(4):681-689.
55. Eggleston ED, Clark RN. Wind speed power spectrum analysis for Bushland, Texas, USA. *Wind Eng*. 2000;24(1):49-52.
56. Soberanis MAE, Mérida W. Regarding the influence of the Van der Hoven spectrum on wind energy applications in the meteorological mesoscale and microscale. *Renew Energy*. 2015;81:286-292.
57. Barnston AG, Livezey RE. Classification, seasonality and persistence of low-frequency atmospheric circulation patterns. *Mon Wea Rev*. 1987;115(6):1083-1126.
58. Aravena J-C, Luckman BH. Spatio-temporal rainfall patterns in southern South America. *Int J Climatol*. 2009;29(14):2106-2120.
59. Peixoto JP, Oort AH. Physics of climate; 1992.
60. Navarra A, Simoncini V. *A Guide to Empirical Orthogonal Functions for Climate Data Analysis*. London & New York: Springer Science & Business Media; 2010.
61. Hannachi A, Jolliffe IT, Stephenson DB. Empirical orthogonal functions and related techniques in atmospheric science: a review. *Int J Climatol*. 2007;27(9):1119-1152.
62. Mahecha MD, Fürst LM, Gobron N, Lange H. Identifying multiple spatiotemporal patterns: a refined view on terrestrial photosynthetic activity. *Pattern Recogn Lett*. 2010;31(14):2309-2317.
63. Garreaud R, Lopez P, Minvielle M, Rojas M. Large-scale control on the Patagonian climate. *J Clim*. 2013;26(1):215-230.
64. Garreaud RD. Cold air incursions over subtropical South America: mean structure and dynamics. *Mon Weather Rev*. 2000;128(7):2544-2559.
65. Vera CS, Vigliarolo PK. A diagnostic study of cold-air outbreaks over South America. *Mon Weather Rev*. 2000;128(1):3-24.
66. Garreaud RD. The Andes climate and weather. *Adv Geosci*. 2009;22:3.
67. Baldwin MP. Annular modes in global daily surface pressure. *Geophys Res Lett*. 2001;28(21):4115-4118.
68. Gong D, Wang S. Definition of Antarctic oscillation index. *Geophys Res Lett*. 1999;26(4):459-462.
69. Marshall GJ. Trends in the southern annular mode from observations and reanalyses. *J Clim*. 2003;16(24):4134-4143.
70. Fogt RL, Perlwitz J, Monaghan AJ, Bromwich DH, Jones JM, Marshall GJ. Historical SAM variability. Part II: twentieth-century variability and trends from reconstructions, observations, and the IPCC AR4 models. *J Clim*. 2009;22(20):5346-5365.
71. Villalba R, Lara A, Masiokas MH, et al. Unusual southern hemisphere tree growth patterns induced by changes in the southern annular mode. *Nat Geosci*. 2012;5(11):793.
72. Sexton DMH. The effect of stratospheric ozone depletion on the phase of the Antarctic oscillation. *Geophys Res Lett*. 2001;28(19):3697-3700.
73. Polvani LM, Kushner PJ. Tropospheric response to stratospheric perturbations in a relatively simple general circulation model. *Geophys Res Lett*. 2002;29(7).
74. Thompson DWJ, Solomon S. Interpretation of recent southern hemisphere climate change. *Science*. 2002;296(5569):895-899.
75. Gillett NP, Thompson DWJ. Simulation of recent southern hemisphere climate change. *Science*. 2003;302(5643):273-275.
76. Shindell DT, Schmidt GA. Southern hemisphere climate response to ozone changes and greenhouse gas increases. *Geophys Res Lett*. 2004;31(18).
77. Arblaster JM, Meehl GA. Contributions of external forcings to southern annular mode trends. *J Clim*. 2006;19(12):2896-2905.
78. Hu Y, Fu Q. Observed poleward expansion of the Hadley circulation since 1979. *Atm Chem Phys*. 2007;7(19):5229-5236.
79. Perlwitz J, Pawson S, Fogt RL, Nielsen JE, Neff WD. Impact of stratospheric ozone hole recovery on Antarctic climate. *Geophys Res Lett*. 2008;35(8):L08714.
80. Son S-W, Tandon NF, Polvani LM, Waugh DW. Ozone hole and southern hemisphere climate change. *Geophys Res Lett*. 2009;36(15):L15705.
81. Son S-W, Gerber EP, Perlwitz J, et al. Impact of stratospheric ozone on southern hemisphere circulation change: a multimodel assessment. *J Geophys Res Atmos*. 2010;115(D3):D00M07.
82. Polvani LM, Waugh DW, Correa GJP, Son S-W. Stratospheric ozone depletion: the main driver of twentieth-century atmospheric circulation changes in the southern hemisphere. *J Clim*. 2011;24(3):795-812.
83. Thompson DWJ, Solomon S, Kushner PJ, England MH, Grise KM, Karoly DJ. Signatures of the Antarctic ozone hole in southern hemisphere surface climate change. *Nat Geosci*. 2011;4(11):741.
84. Fyfe JC, Boer GJ, Flato GM. The Arctic and Antarctic oscillations and their projected changes under global warming. *Geophys Res Lett*. 1999;26(11):1601-1604.
85. Kushner PJ, Held IM, Delworth TL. Southern hemisphere atmospheric circulation response to global warming. *J Clim*. 2001;14(10):2238-2249.
86. Cai W, Whetton PH, Karoly DJ. The response of the Antarctic oscillation to increasing and stabilized atmospheric CO_2. *J Clim*. 2003;16(10):1525-1538.
87. Marshall GJ, Stott PA, Turner J, Connolley WM, King JC, Lachlan-Cope TA. Causes of exceptional atmospheric circulation changes in the southern hemisphere. *Geophys Res Lett*. 2004;31(14):L14205.

88. Wan Y-H, Parsons BK. Factors relevant to utility integration of intermittent renewable technologies. NREL/TP-463-4953, Golden, CO (United States), National Renewable Energy Lab.; 1993.

How to cite this article: Bianchi E, Solarte A, Guozden T. Spatiotemporal variability of the wind power resource in Argentina and Uruguay. *Wind Energy*. 2019;22:1086–1100. https://doi.org/10.1002/we.2342